J Inorg Organomet Polym (2017) 27:1252–1263
DOI 10.1007/s10904-017-0573-1

Thione-Based Nickel(II) Complexes as Functional Antioxidant Mimics: Scavenging Activity of Reactive Oxygen Species $O_2^{-\cdot}$ and X-Ray Crystal Structure of $[Ni(Tt^{xyly})_2]_2$ {Tt^{xylyl} = Hydrotris(2-mercapto-1-xylyl-imidazolyl)borate}

Mohamed M. Ibrahim[1,2] · Abd El-Motaleb M. Ramadan[2] · Shaban Y. Shaban[2] · Gaber A. M. Mersal[1,3] · Mohamed M. Soliman[4] · Salih Al-Juaid[5]

Received: 21 February 2017 / Accepted: 4 May 2017 / Published online: 16 May 2017

Abstract Two new thione-based nickel complexes, viz., $[Ni(Tm^{ipr})_2Cl_2]\cdot 2H_2O$ **1** and $[Ni(Tt^{xyly})_2]\cdot H_2O\cdot 2CH_3OH$ **2** {Tm^{ipr} = 1-(2-isopropylphenyl)-1H-imidazole-2(3H)-thione; Tt^{xylyl-} = hydrotris[1-(2,6-dimethylphenyl)-1H-imidazole-2(3H)-thione]borate anion} have been synthesized. Their structures and properties were characterized by several physicochemical methods, namely elemental and thermal analysis, FT-IR and Raman and UV–Vis spectroscopes, as well as electrical molar conductivity measurements. Structural determination of complex **2** showed that the coordination geometry around nickel atom is distorted tetrahedral with four thione sulfur donors from two molecules of the ligand KTt^{xylyl}. Steric interactions between the xylyl rings appear to be responsible for the formation of the mononuclear nickel(II) complex **2**. Molecules of complex **2** are connected via S–H···O hydrogen bonds, involving hydrogen atoms of the coordinated thiones and lattice water molecules. The *superoxide dismutase* biomimetic catalytic activities of both complexes were tested and found to be promising candidates as functional mimic enzyme to serve for complete superoxide radical's detoxification. The observed IC_{50} values of these complexes are 8.38 and 7.4 mM for complexes **1** and **2**, respectively.

Keywords Thione-based nickel(II) complexes · X-ray structure · Biomimetic · Redox enzymes · Antioxidants

1 Introduction

As a result of scientific progress and development of means of measurement, new concepts have recently emerged. The most famous of these concepts are so-called sports corrosion, chemical terrorist or biological traitor. Despite the benefits of exercising physical activity to the body, yet it leads to the formation of the so-called free roots or radicals ($O_2^{-\cdot}$) [1–3]. This reduced form of oxygen molecule may lead to oxidation of the key elements of the cell, and therefore it damages, deaths or the corruption of DNA if not resisted [4]. These radicals interact with each other to produce the most serious picture including the interaction of superoxide anion ($O_2^{-\cdot}$) with nitric oxide, to produce peroxide, nitrite [5, 6], as well as the interaction of superoxide anion with fat to form its different radicals [7, 8]. So it becomes clear that the solution lies in antioxidants or oxidation inhibitors which are body materials to prevent damage of free radicals and also work to prevent muscle soreness or muscle damage. Antioxidants have gained considerable attention in nowadays because of its role in anti-aging [9], cancer [10], heart disease and many other health problems [11].

Various scientific studies have proved that people who suffer from these diseases, they also suffer from a rise in the

Electronic supplementary material The online version of this article (doi:10.1007/s10904-017-0573-1) contains supplementary material, which is available to authorized users.

✉ Mohamed M. Ibrahim
ibrahim652001@yahoo.com

[1] Chemistry Department, Faculty of Science, Taif University, Taif, Saudi Arabia

[2] Department of Chemistry, Faculty of Science, Kafrelsheikh University, Kafr El-Sheikh 33516, Egypt

[3] Department of Chemistry, Faculty of Science, South Valley University, Qena, Egypt

[4] Biochemistry Department, Faculty of Veternary Medicine, Benha University, Benha, Egypt

[5] Chemistry Department, Faculty of Science, King Abdulaziz University, Jeddah, Saudi Arabia

concentration of superoxide radicals incision accompanied by deficiency in superoxide enzymes [12]. Consequently, specialists have reached the idea of overcoming this problem by giving superoxide enzymes for these infected cases. Unfortunately, this process did not succeed because of the difficulty of trading and dealing with this protein due to its sensitivity and vulnerability of surrounding circumstances and therefore its damage. And this also happens because the natural enzymes (which have been drawn with difficulty from some other organisms such as bacteria and pork) have large molecular weights and cannot pass through the cell membrane and thus have a local impact.

More recently a mononuclear nickel cofactor containing SOD has been identified in Streptomyces and marine cyanobacteria [13]. X-ray crystallographic studies of the reduced and oxidized forms of the Ni-SOD enzyme from *Streptomyces seoulensis* and *Streptomyces coelicolor* have revealed that the active site of the metalloenzymes (this nickel(II) protein) contains cysteine–thiolate coordination at the nickel centre [14]. The SOD reaction involves the binding of superoxide to the Ni^{2+} center, generating a Ni^{2+}-peroxo species that undergoes proton and electron transfer to generate H_2O_2 and the oxidized Ni^{3+} center. Binding of a second superoxide generates a Ni^{3+}-peroxo intermediate, which donates an electron back to the Ni^{3+} center to liberate dioxygen and re-form the starting Ni^{2+} state [15–17].

So, the idea of getting synthesized mimic compounds similar in activity to the superoxide dismutase enzyme [18–22] has appeared and succeeded for the following reasons: (i) these compounds have small molecular weights and can pass through the cell membrane and access to the defected places that natural enzymes cannot get accessible [23], (ii) these compounds can be synthesized in appropriate and plentiful amounts, (iii) the stability of these compounds toward the surrounding circumstances and the easiness of handling and dealing with, (iv) catalytic activity of these compounds can be allow them to act as a superoxide dismutase enzyme [24].

As part of our on-going research on the biological activities of several mononuclear nickel(II) and copper(II) complexes [25–30] and in view of the potential that model(II) complexes possess to catalytically destroy the highly reactive, destructive and toxic superoxide radical anion, $O_2^{-\cdot}$ to H_2O_2 and O_2, the main lines of our proposed research are: (i) Design and synthesis of two new thione-based nickel complexes, viz., $[Ni(Tm^{ipr})Cl_2]$ **1** and $[Ni(Tt^{xylyl})_2]$ **2** (Tm^{ipr} = 2-mercapto-1-isopropylimidazole; Tt^{xylyl} = hydrotris(2-mercapto-1-xylyl-imidazolyl)hydroborate); (ii) The relationship between the geometry (the available coordination sites) of the complexes and the catalytic activity towards toxic superoxide radical anion, $O_2^{-\cdot}$, will be examined, (iii) Research into the structure of these model complexes by means of X-ray structure determinations (XRC and XRD) for a better understanding of structure–activity relationships. We will bring together our expertise in destroying the highly reactive, destructive and toxic superoxide radical anion, $O_2^{-\cdot}$ to H_2O_2 and O_2, using these nickel(II) model complexes as structural mimics for the active sites of antioxidant enzyme, SOD.

2 Experimental

2.1 Materials and Methods

All chemicals used were of analytical grade. The ligands 2-mercapto-1-xylylimidazole (Tm^{ipr}) and tris(2-mercapto-1-xylyl-imidazolyl)hydroborate (Tt^{xylyl}) were synthesized by our previously published methods [31–35]. The IR spectra were recorded using Alpha-Atunated FT-IR Spectrophotometer, Bruker in the range of 400–4000 cm^{-1}. The elemental analyses of compound **1** was measured using Perkin-Elmer Series II CHNS/O Analyzer 2400. Raman spectra were recorded Bruker FT-Raman with laser. The spectra were recorded at room temperature with a germanium detector, maintained at liquid nitrogen temperature and using 1064.0 nm radiation, generated by a Nd–YAG laser with a resolution of 2 cm^{-1}. The conductivity measurements were carried out using Equiptronics digital conductivity meter model JENWAY 4070 type at room temperature for (1×10^{-3} mol L^{-1}) solutions. All UV–Vis measurements were recorded by a UV-Lambda 25 Perkin Elmer. Thermal analyses of the complexes were recorded on Shimadzu DTG 60H with system interface device in the atmosphere of nitrogen. The operational range of the instrument was from ambient temperature to 600 °C. Accurately 15 mg of pure sample was subjected for dynamic TG scans at heating rate of 10 °C min^{-1}.

2.2 Syntheses

2.2.1 *Synthesis of Dichlorobis(2-Mercapto-1-xylylimidazole) Nickel(II)* ***1***

A warm solution of $NiCl_2{\cdot}6H_2O$ (0.47 g, 2 mmol) in 10 mL of methanol was added to a warm solution of 2-Mercapto-1-xylylimidazole, Tm^{xylyl} (0.87 g, 4 mmol) in 10 mL methanol. The resulting mixed solution was stirred for 10 h at room temperature. The volume of the solution was reduced to 5 mL in vacuo, and the precipitate was filtered off and dried. Orange crystals were obtained by slow evaporation of methanolic solution of $[Ni(Tm^{ipr})_2Cl_2]{\cdot}2H_2O$ **1**. Anal. For $C_{24}H_{32}Cl_2N_4O_2S_2Ni$ (602.28): Calcd.: C, 47.86; H, 5.36; N, 9.30; Cl, 11.77; S, 10.56; Ni, 9.75. Found: C,

47.33; H, 5.44; N, 9.46; Cl, 12.01; S, 10.30; Ni, 9.63. IR-ATR: ν (cm^{-1}): 3350 [m, br, OH], 3180 [s, br, NH], 1572 [s, –C=C–+ C=N], 1465 [s, thioamide I], 1291 [w thioamide II], 1110 [w, thioamide III], 735 and 678 [s, thioamide IV], 666 [w, δ (C=S)] and 505 [s, π (C=S)].

2.2.2 *Synthesis of bis{Hydrotris[N-(2,6-xylyl)-2-thioimidazol-1-yl] borato}nickel(II)* **2**

A solution of $Ni(NO_3)_2{\cdot}6H_2O$ (87 mg, 0.3 mmol) in 5 mL of methanol was added drop wise to a solution of KTt^{xylyl} (200 mg, 0.3 mmol) in 5 mL methanol. The resulting mixed solution was stirred for 6 h at room temperature. The resulting nickel(II) complex was extracted from CH_2Cl_2, The volume of the solution was reduced to 5 mL in vacuo, and the precipitate was filtered off and dried. Single crystals of $[Ni(Tt^{xyly})_2]{\cdot}H_2O{\cdot}2CH_3OH$ 2, suitable for X-ray measurement were obtained. Anal. For $C_{68}H_{78}B_2N_{12}O_3S_6Ni{\cdot}$ (1384.14): Calcd. C, 59.01; H, 5.68; N, 12.14; S, 13.90; Ni, 4.24. Found C, 58.83; H, 5.74; N, 12.05; S, 13.81; Ni, 4.29. IR-ATR: ν (cm^{-1}): 3400 [w, br, OH], 2446 [w, B–H], 1635 [s, –C=C–], 1590 [w, –C=N–], 1041 and 1018 [w, ν (C=S)], 957 and 888 [w, ν (–C–S–)], 689 [w, δ (C=S)], 610 [s, π (C=S)] and 524 [w, δ (–C=C–)].

Table 1 Sample and crystal data of nickel(II) complex **2**

Chemical formula	$C_{68}H_{78}B_2N_{12}NiO_3S_6$	
Formula weight	1384.11	
Temperature	100(2) K	
Wavelength	0.71073 Å	
Crystal size	0.180 × 0.200 × 0.220 mm	
Crystal system	Monoclinic	
Space group	P 1 21/c 1	
Unit cell dimensions	a = 13.8597(9) Å	α = 90°
	b = 20.3754(14) Å	β = 94.493(2)°
	c = 25.6965(18) Å	γ = 90°
Volume	7234.3(9) $Å^3$	
Z	4	
Density (calculated)	1.271 g cm^{-3}	
Absorption coefficient	0.494 mm^{-1}	
F(000)	2912	

2.3 X-Ray Single Crystal and Powder Diffraction Determinations

The crystallographic data (Table 1) were collected on a Smart-CCD diffractometer of Bruker AXS using Mo-Kα radiation. None of the crystals show significant intensity loss throughout the data collections (Table 2). Lorentz-Polarisation corrections were performed by SAINT [36]. Absorption corrections were made by using the SADABS program [37]. The structures were solved by direct or Patterson methods using SHELXS-97 [38] to find out the position of the heavy atoms. The other non-hydrogen atoms were located by Fourier syntheses and refined using SHELXS-97 [38]. The least squares refinements were performed using all independent reflections by the full matrix on F2. The hydrogen atoms were positioned at calculated sites (with C–H 0.96 Å) and were constrained to ride on their linked atoms with isotropic thermal parameters of 1.5 times the factor of the methyl groups and 1.2 times

Table 2 Data collection and structure refinement of nickel(II) complex **2**

Theta range for data collection	1.28°–28.30°	
Index ranges	$-18 \le h \le 18$, $-27 \le k \le 27$, $-34 \le l \le 30$	
Reflections collected	72,648	
Independent reflections	17,928 [R(int) = 0.0741]	
Max. and min. transmission	0.9160 and 0.8990	
Structure solution technique	Direct methods	
Structure solution program	SHELXS-97 (Sheldrick, 2008)	
Refinement method	Full-matrix least-squares on F^2	
Refinement program	SHELXL-2013 (Sheldrick, 2013)	
Function minimized	$\Sigma w(F_o^2 - F_c^2)^2$	
Data/restraints/parameters	17,928/3/851	
Goodness-of-fit on F^2	1.012	
Δ/σ_{max}	0.464	
Final R indices	11,689 data; $I > 2\sigma(I)$	R1 = 0.0625, wR2 = 0.1379
	All data	R1 = 0.1101, wR2 = 0.1571
Weighting scheme	$w = 1/[\sigma^2(F_o^2) + (0.0637P)^2 + 10.6979P]$ where $P = (F_o^2 + 2F_c^2)/3$	
Largest diff. peak and hole	1.113 and −0.596 e$Å^{-3}$	
R.M.S. deviation from mean	0.084 e$Å^{-3}$	

the factor of the other groups. X-ray diffraction patterns (XRD) were measured using Bruker D8-advance diffractometer (Cu $K\alpha_1$-radiation) in the scan range 2h = 20°–90°. For instrumental broadening correction, LaB_6 standard was used. The crystal structure and microstructure were analyzed applying Rietveld method, using MAUD program [39].

2.4 SOD-Like Activity Study

The super oxide dismutase (SOD) mimetic activity of the synthesized complexes 1 and 2 at variable concentrations (from 1 to 10 mM) were determined by Nitroblue Tetrazolium/reduced Nicotinamide/Phenazine methosulphate (NBT/NADH/PMS) system [40–42]. The amount of reduced NBT was recorded spectrophotometrically at 560 nm by monitoring the increase in the concentration of blue formazan form for 5 min. The reaction in blank samples and in the presence of nickel(II) complexes was measured for 5 min of incubation. Experiments were repeated three times to ensure consistency of the results. Data were analyzed using analysis of variance (ANOVA) and post-hoc descriptive tests by SPSS software version 11.5 for Windows with $p < 0.05$ regarded as statistically significant. Regression analysis was performed using the same software.

3 Results and Discussion

3.1 Characterization of the Model Complexes 1 and 2

The reaction of the ligand Tm^{ipr} with nickel(II) chloride in 2:1 molar ratio in methanol readily produced the crystalline complex $[Ni(Tm^{ipr})_2Cl_2]\cdot 2H_2O$ **1**. On the other hand, the reaction of KTt^{xylyl} with nickel(II) nitrate hexahydrate in 1:1 molar ratio in hot methanol readily afforded the crystalline nickel(II) complex $[Ni(Tt^{xyly})_2]\cdot H_2O\cdot 2CH_3OH$ **2** in good yield (Scheme 1). The elemental analysis of both complexes confirmed their stoichiometry. In order to establish the mode of coordination for both complexes, we have examined their IR and Raman spectroscopes, as well as thermal analysis and electrochemical measurements, including cyclic voltammetry. The molar conductivities are 11.82 and 15.1 Ω^{-1} cm^2 mol^{-1} for complexes **1** and **2**, respectively commensurate with the non-electrolytic behaviors of both complexes [43]. Thermal analysis data have further confirmed the results of elemental analyses. The identity of compound **1** was also confirmed by EI-MS, which shows the presence of the expected nickel(II) compound **1** with an *m/e* centered around 666 amu. The molecular structure determination of complex **2** showed that the nickel atom is coordinated to four thione sulfur atoms (S_4), from two ligand systems, leaving two thiomidazolyl thione sulfure donors away from the coordination sphere.

3.2 IR and Raman Spectra

The IR spectrum of nickel(II) complex **1** shows the absence of ν(SH) band at ~2500 cm^{-1} and the presence of ν(NH) band in the range of 3185–3170 cm^{-1}, as well as shifts to lower frequency in the ν(C=S) absorption to 505 cm^{-1}. This clearly indicates that the ligand is coordinated via the thione sulfur atoms in both complexes [44]. These shifts may result from (i) changes in the electronic state where the C=S bond loses some of its double bond character when the ligand coordinates *via* the thione sulfur and (ii) hydrogen bond effects, where it is a common feature of

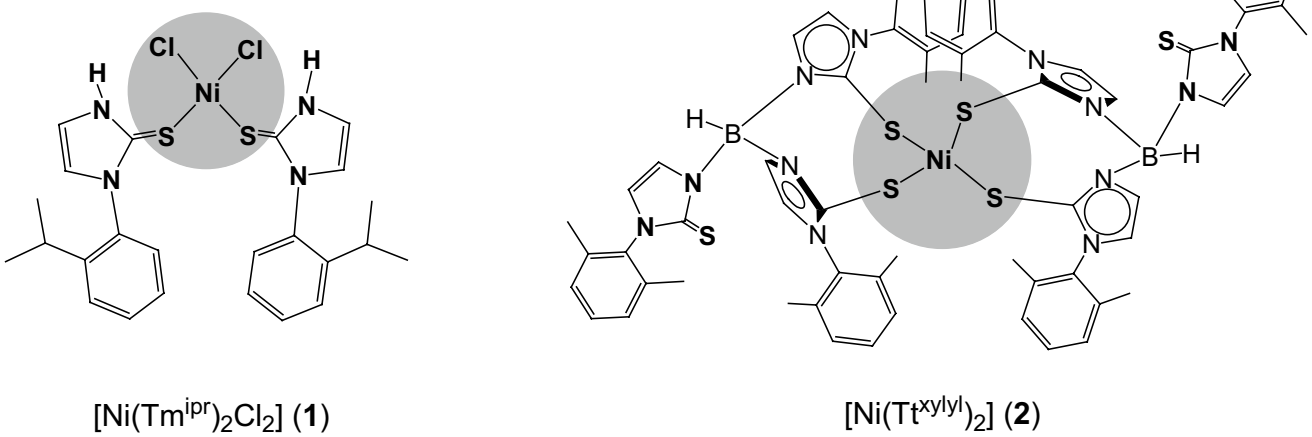

Scheme 1 The structures of the model complexes **1** and **2**

1-methylimidazoline-2(3H)-thione complexes in which the thioamide proton (N(1)–H) of the molecule acts as an effective H-bond donor atom [45]. All of the thioamide bands are shifted to some degree, but the most significant change is that observed in the thioamide IV bands, which have the largest shift to lower frequency [46, 47]. The thioamide IV band is affected with the bands in the free ligand (757 and 728 cm^{-1}), which are replaced by a sharp band at 735 and 678 cm^{-1} for nickel(II) complex **1**. The IR spectrum of complex **2** (Fig. 1) showed a single ν(B–H) absorption at 2246 cm^{-1} shifted around 100 cm^{-1} to lower energy relative to that of the free ligand [31–35]. Given the fact that the coordination of B–H bonds to transition metals characteristically leads to lower B–H stretching frequencies [48–50], this change in the IR absorption band is likely due to the existence of an interaction between the nickel and B–H centers, which may lead to B–H···Ni interactions. Similar type of interactions has also been observed for analogous monomeric [51–53] and dimeric [54–57] structures. The presence of two very intense bands at 1041 and 1018 cm^{-1} was assigned as C=S terminal stretching. These bands are generally used to confirm the presence of Tt^{xylyl} ligand in complex **2**. Other assignments are: bands at 957 and 888 cm^{-1} to C–S stretches, the low intensity band at 524 cm^{-1}, a breathing mode of the heterocyclic Tt^{xylyl} complex, and the bands below 500 cm^{-1}, to angular deformation and Ni–S stretching modes. These shifts may result from changes in the electronic state where the C=S bond loses some of its double bond character when the ligand coordinates via the thione sulfur. The shifts in the bands between the free ligand and the complexes result from electronic shifts within the ligand. In the –OH stretching region, a

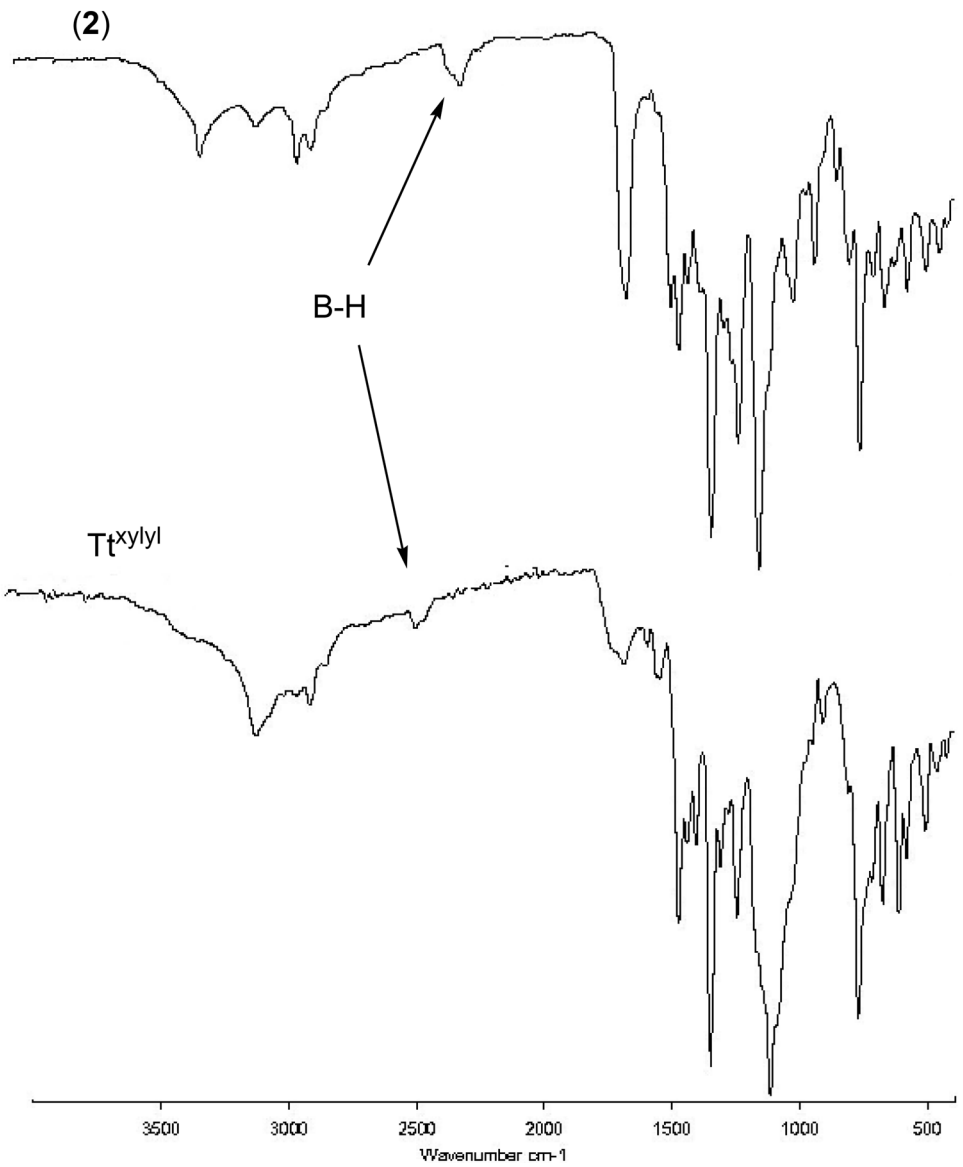

Fig. 1 FT-IR spectra of the ligand Tt^{xylyl} and its nickel(II) complex **2**

very broad absorptions in the range of 3300–3400 cm^{-1} are detected for lattice water molecules in both complexes [58]. Information about the low frequency nickel(II)–S(thionate) vibrations can be obtained by using Raman spectroscopy. Typical Raman spectra obtained for the ligand Tt^{xylyl} and its nickel(II) complex **2** is shown in Fig. 2. The band of most interest is the one formed upon complexation, which must therefore be the result of nickel(II)–thione(S) bonding. In the spectrum shown, prominent new bands include the strong peaks around 251 and 173 cm^{-1} for the 1:1 complex with the ligand Tt^{xylyl}, which we conclude that the result of the formation of nickel(II)–ligand bonds through the sulfur atom.

3.3 Magnetic Moment and Electronic Absorption Spectra

At room temperature the present four-coordinated nickel(II) complexes show magnetic moment in the range 3.15–3.28 BM corresponding to two unpaired electrons. These values are in tune with a high spin configuration and show the presence of a tetrahedral environment [59, 60] around the nickel(II) ion in the inspected complexes. So, these magnetic moment values demonstrate that these nickel(II) complexes are paramagnetic and have a high spin tetrahedral configuration with $^3T_1(F)$ ground state [59, 60]. These paramagnetic properties of the four coordinate nickel(II) complexes confirm the sp^3 hybridization of nickel(II) ion in a tetrahedral environment while the dsp^2 hybridization of square planar stereochemistry is remote.

The electronic spectra of the present four-coordinated nickel(II) complexes in DMF solution exhibit three absorption bands in the range 499–510, 590–605 and 680–690 nm. The general feature of the spectra of these two complexes is similar to each other and suggests that the coordination structure of these two complexes is almost analogous. An examination of these bands indicates that the complexes have a tetrahedral geometry and the ground stat of nickel(II) ion in a tetrahedral geometry is $^3T_1$ [61]. Thus, these bands may be assigned to the three spin allowed transitions [58]: $^3T_1(F) \rightarrow {}^3T_2(F)$ (ν_1), $^3T_1(F) \rightarrow {}^3A_2$ (ν_2) and $^3T_1(F) \rightarrow {}^3T_1(P)$ (ν_3) respectively. In the regular tetrahedral and near-tetrahedral nickel(II) complexes only one d–d transition is observed in the visible region. The three closely spaced transitions in the spectra of the inspected nickel(II) complexes arise from the distortion in the tetrahedral symmetry around the nickel(II) center. This splitting originates from the reduction of the orbital degeneracy due to the difference in the ligand field strength of sulfur atoms and halides donor atoms for complex **1** and the restricted bite angle of the S(1)–M–S(2) chelating ligand. The reported electronic spectral data conform to the

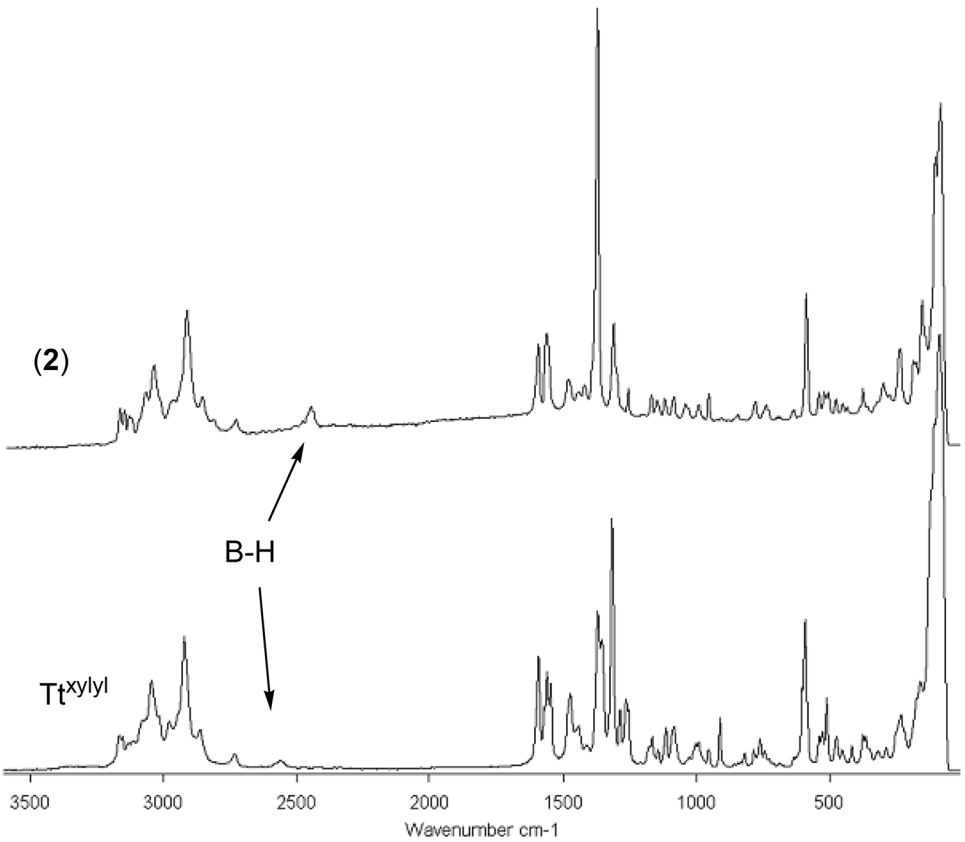

Fig. 2 Raman spectra of the ligand Tt^{xylyl} and its nickel(II) complex **2**

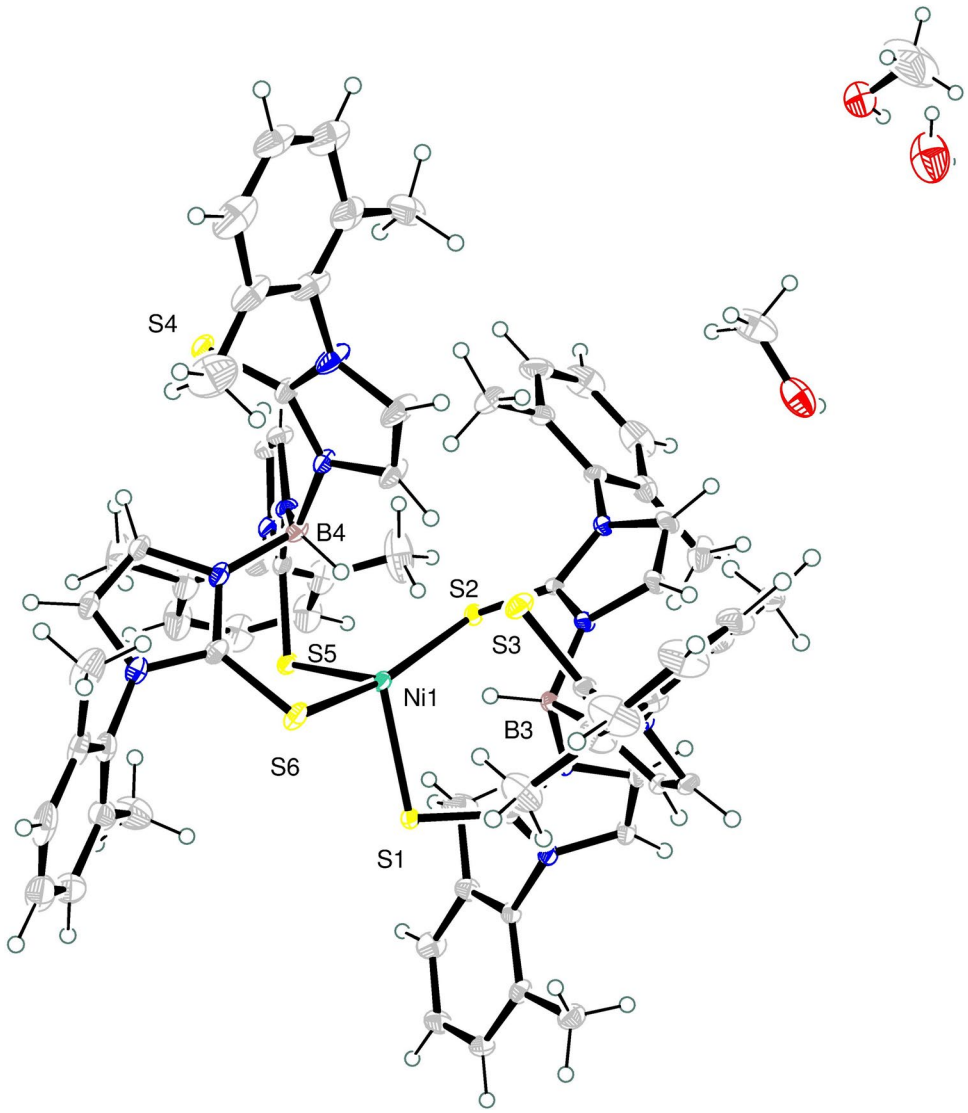

Fig. 3 Solid presentation of single crystal X-ray structure of copper(II) complex **2**, showing the labeling scheme of non-hydrogen atom

structure determined by X-ray crystallography for complex 2. This spectral behavior is comparable with analogous tetrahedral nickel(II) complexes [62, 63]. Hence the nickel(II) ion of the present nickel(II) complexes has sp^3 hybridization of the tetrahedral geometry. The intensity of the UV-band around 330 nm is consistent with its being a ligand-centered $\pi \rightarrow \pi^*$ transition or a charge-transfer transition.

3.4 Crystal Structure Determinations

Nickel(II) complex **2** crystallizes as a monomer in monoclinic crystal system in the space group P-1. An ORTEP representation of complex **2** is shown in Fig. 3 and selected bond lengths (Å) and angles (°) are included in Table 3. The structure determination of nickel(II) complex **2** revealed that the ligand Tt^{xylyl} acts as a bidentate sulfur donors, i.e. one of the thioimidazolyl arms of the tripod is away of coordination. This corresponds to the observations made

Table 3 Bond lengths (Å) and angles (°) of nickel (II) complex **2**

Bond lengths (Å)			
Ni1–S6	2.3567(9)	Ni1–S1	2.3634(8)
Ni1–S2	2.3798(9)	Ni1–S5	2.4070(10)
B3–N5	1.528(5)	B3–N3	1.537(4)
B3–N1	1.558(4)	B3–H3A	1.0
Bond angles (°)			
S6–Ni1–S1	87.51(3)	S6–Ni1–S2	162.60(3)
S1–Ni1–S2	106.14(3)	S6–Ni1–S5	101.06(3)
S1–Ni1–S5	100.60(3)	S2–Ni1–S5	87.22(3)
C1–S1–Ni1	99.72(10)	C61–S2–Ni1	108.42(11)
C50–S5–Ni1	103.17(12)	C30–S6–Ni1	100.46(12)
N1–B3–H3A	110.2	N5–B3–N3	108.9(3)
N5–B3–N1	110.4(2)	N3–B3–N1	106.8(3)
N5–B3–H3A	110.2	N3–B3–H3A	110.2

Table 4 Hydrogen bond distances (Å) and angles (°) of nickel(II) complex **2**

	Donor–H	Acceptor–H	Donor–acceptor	Angle
C3–H3···O2	0.95	2.44	3.360(5)	164.6
C39–H39···S3	0.95	2.7	3.412(4)	131.8
C40–H40···S4	0.95	2.74	3.367(3)	124.3
C41–H41···O2	0.95	2.44	3.345(5)	158.5
C62–H62···O1	0.95	2.38	3.257(5)	153.3
C65–H65···S4	0.95	2.91	3.624(3)	132.6
C67–H67···S4	0.95	2.9	3.498(4)	121.9
O1–H1···S1	0.84	2.67	3.502(3)	172.8
O2–H2A···O3	0.84	1.97	2.813(6)	176.3
O3–H4W···S3	0.835(11)	2.74(7)	3.295(5)	125.0

previously for similar $Zn(Tt)_2$ complexes [64–67] The complex shows that the Ni–S bond lengths ranging from 2.36 to 2.41 Å and its very wide spread of S–Ni–S angles resemble those in the known complexes, which show quite a range around the tetrahedral angle, the extremes being 89° in complex **2**. Steric interactions between the xylyl rings to be responsible for the formation of mononuclear tetrahedral nickel(II) complex **2** [68]. In complex **2**, the ligand molecules have their S(1)C(1)N(1)N(2) moieties essentially planar and have similar bond distances: S(1)–C(3) 1.712(3) A°, N(1)–C(1) 1.350(4) A°, and N(2)–C(1) 1.35272(4) A°. The bond distances reported for the free imidazolinethiol molecule are d(S–C): 1.677(4) A°, d(N–C): 1.330(3) and 1.329(4) A° [21]. On average, the C=S distance is increased from 1.703 A°, in the free ligand to 1.693 A° in complex **2**. This is consistent with a partial reduction of p-character of the C=S bonds in the coordinated ligands and thus a decrease of the C=S distance relative to the main free ligand distance [69]. This indicates that the C=S bonds are double bonds, as in the free ligand. The structure shows the presence of extensive intermolecular hydrogen bonding interactions (Table 4; Fig. 4). The hydrogen atoms of the axial chloride ligand is hydrogen bonded with the hydrogen atoms belonging to the water molecules (distance ~2.3 Å) (Table 4). A view of the packing of **2** is shown in Fig. 2 illustrating the π···π interactions between xylyl rings.

Figure 5 shows the difference between nickel complexes **1** and **2** where the diffraction patterns are totally different. Structure characterization of the materials have been made by employing the Rietveld's whole profile fitting method based on structure refinement using the MAUD 2.044 software [70]. The idea behind the *Rietveld* method

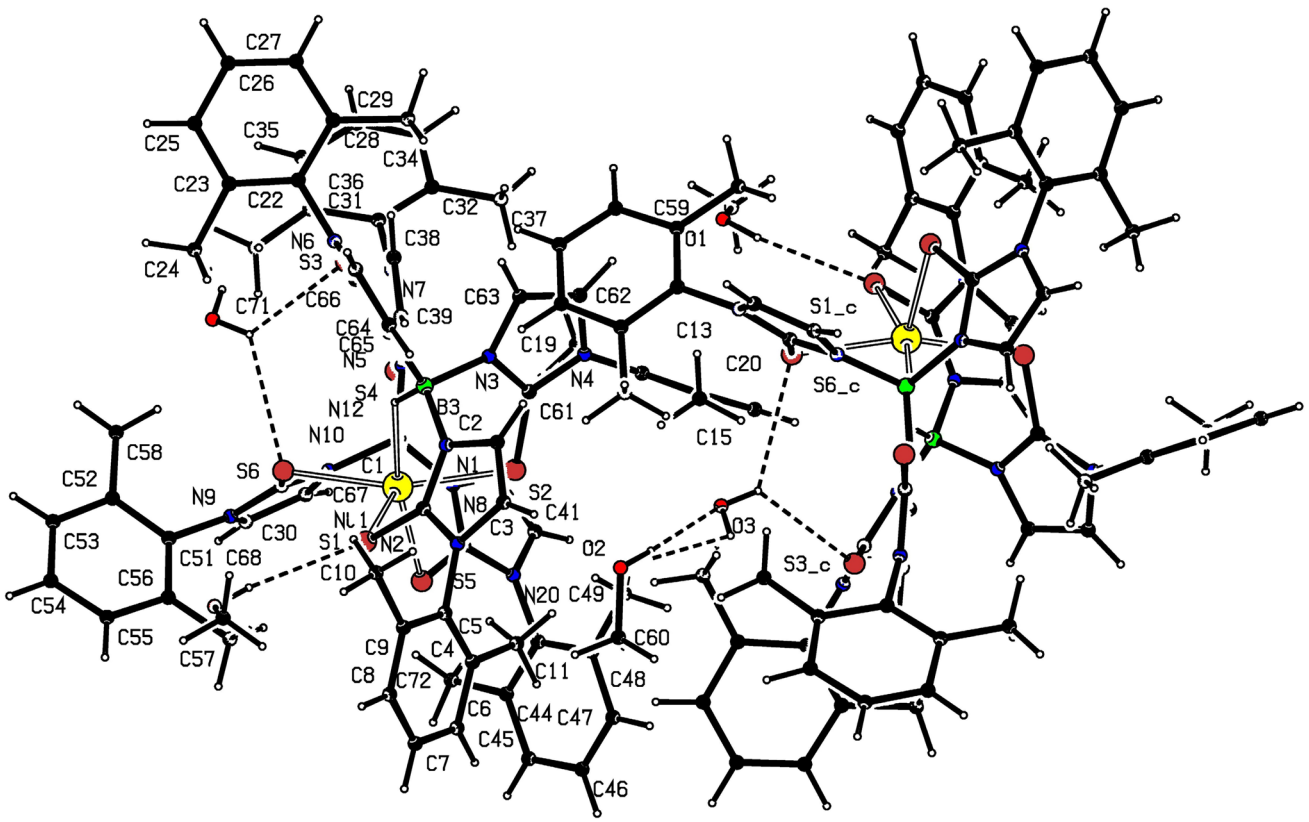

Fig. 4 Projection along *c* axis, describing the geometry in the ribbons which are formed from the copper(II) complex **2**. Inter and intra hydrogen bonding displayed

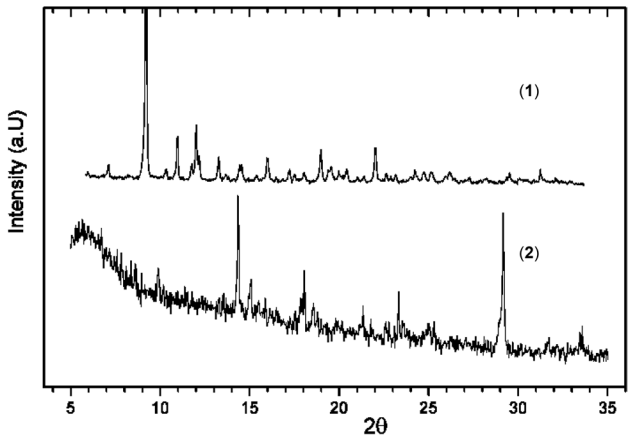

Fig. 5 X-ray diffraction patterns of nickel(II) complexes **1** and **2**

is to consider the entire powder diffraction pattern using a variety of refinable parameters. The basic idea is to calculate the entire powder pattern using a structural model with variety of refinable parameters and to improve a selection of these parameters by minimizing the weighted sum of the squared differences between the observed and calculated pattern using least squares methods.

3.5 Thermal Analysis

The thermal analysis measurements indicate that the decomposition of the newly synthesized complexes **1** and **2** proceeds in several stages. The TG-DTA thermogram of complex **1** (Fig. 6) exhibits an endothermic event at 405 K accompanied by a mass loss of 5.97% (calc. 6.40%), assigned to the removal of two lattice water molecules. This stage is followed by three decomposition processes as evidenced by the strong endothermic and exothermic characteristic peaks at 498, 725 and 874 K, respectively. Two-third of the ligand molecules as well as two chlorine atoms (Calc. 59.16%; Found 57.00%) were lost in the second and third stages and the remainder was lost in the final stage of the decomposition, forming a mixture of NiO+2C as final solid products (Calc. 16.39%; Found 16.08%). As shown in Fig. 7, the pyrolysis of complex **2** exhibits an endothermic event at 410 K, accompanied by a mass loss of 6.29% (calc. 5.92%), assigned to the removal of the latticed water and methanol molecule. This step is followed by three decomposition processes as evidenced by the strong endothermic and exothermic events at 540, 756 and 875, respectively, attributable to complete removal of the remaining organic ligand leaving behind a mixture of Ni_2O_3+B_4C as a final residual (Calc. 15.94%; Found 15.63%).

3.6 SOD Activity

It has been reported that superoxide anion radical and the other related radicals may contribute significantly to sustaining chronic inflammation by promoting connective tissue degradation [71, 72]. In this context, nickel(II) complexes exhibit SOD like activity are promising candidates for treatment the inflammatory diseases. This anti- inflammatory action has been related to facilitation of lysyl oxidase activity required for the repair connective tissue components and either SOD–mimetic activity of the

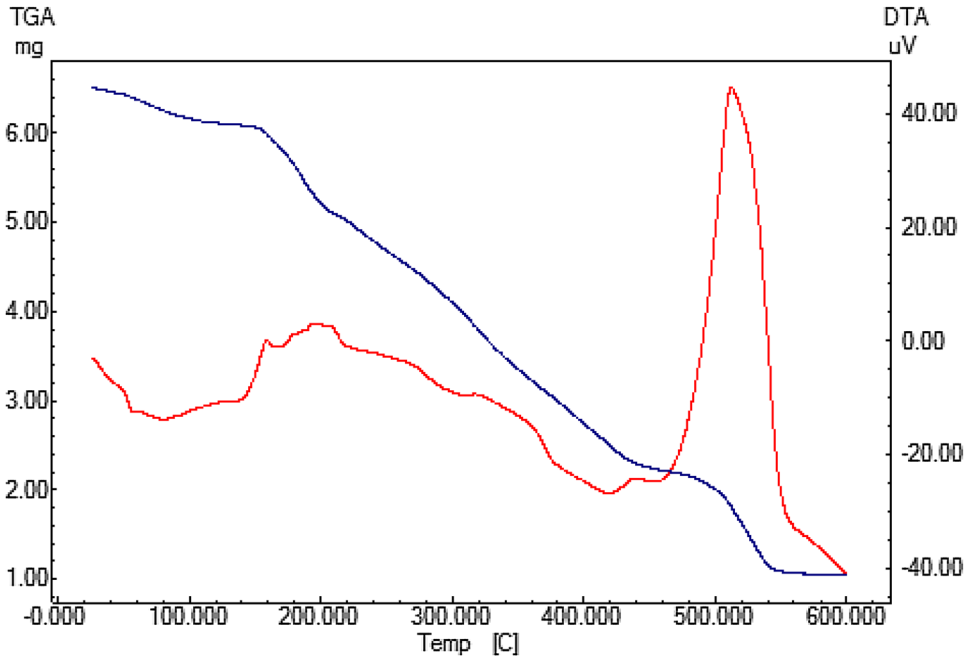

Fig. 6 TGA-DTA thermograms of nickel(II) complex **1**

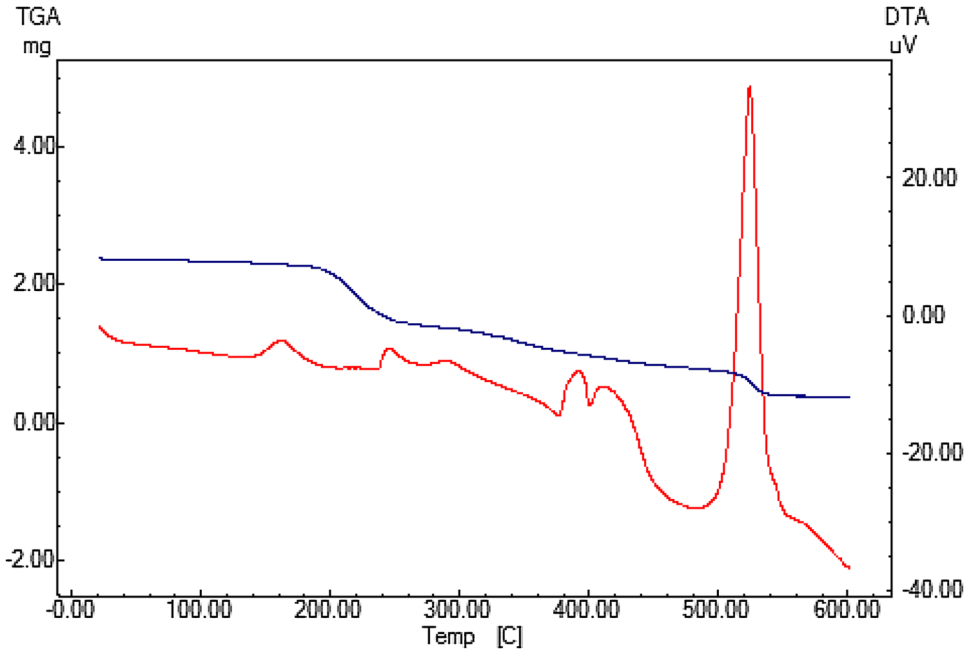

Fig. 7 TGA-DTA thermograms of nickel(II) complex **2**

administered complexes or their facilitation of Ni–SOD synthesis. Therefore, it is interesting to investigate the SOD-like activity of these new nickel(II) complexes. SOD mimetic activity of the present nickel(II) complexes which was evaluated by their scavenging ability have been determined and the obtained results demonstrate valuable SOD-like activity of the inspected nickel(II) chelates. The observed IC_{50} values of the present nickel(II) chelates are comparable with the earlier reported for copper(II) complexes [73]. The catalytic activity of NiSOD [74], however, is on the same high level as that of Cu, ZnSOD at about 109 M^{-1} s^{-1} per metal center. Figure 8 showed the ability for the inhibition% of these complexes at different concentrations. As shown in Table 5, both complexes **1** and **2** showed SOD as functional unites and both have dose dependant effect on SOD activity. The observed IC_{50} values of these complexes are 8.38 and 7.4 mM for complexes **1** and **2**, respectively. These results indicated that complex **1** is more reactive than complex **2**. The SOD-like activity of some metal complexes is a function of several factors, among them is the exchange ability of the axial coordinated ligand, the steric hindrance and flexibility of the metal ion

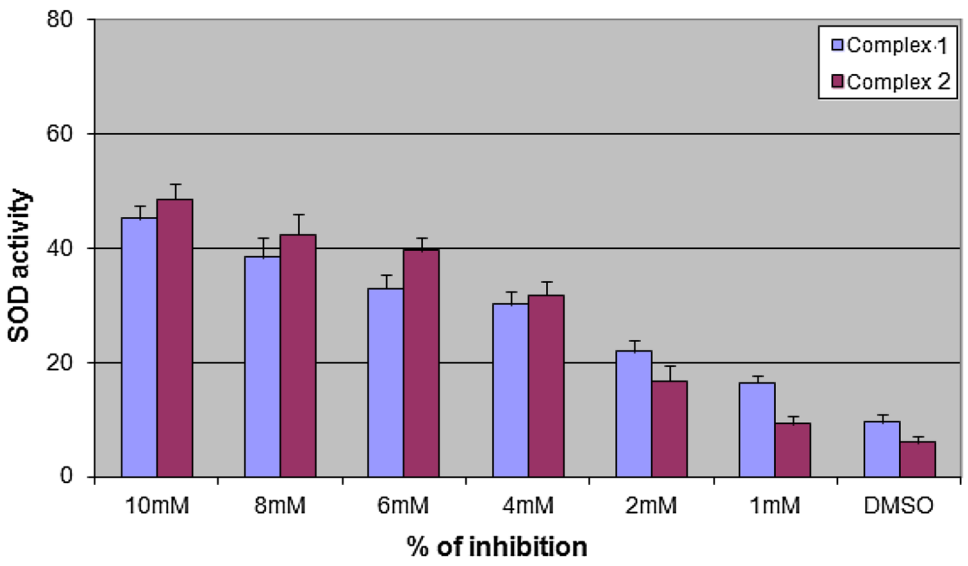

Fig. 8 SOD-like activity of complexes **1** and **2**. SOD activity was measured for complexes as stated in materials and methods at different concentrations (1–10 mM) and in DMSO as a solvent. SOD activity is expressed as U L^{-1}

Table 5 The levels of SOD as functional unites

Complex	SOD	
	Concentration (mM)	Activity (U L^{-1})
Purified SOD	1.5 unit per assay	200[a]
(1)	1	57.4
	2	76.7
	4	105.47
	6	115.06
	8	134.2
	10	158.2
(2)	1	32.3
	2	58.3
	4	111.3
	6	138.4
	8	148.4
	10	169.6

[a]Based on SOD kits used for measurement of SOD activities, 1.5 unite of purified SOD was shown to induce 80% inhibition (functional units; 200 U L^{-1} as stated in this table [40]). Used kits were imported from Biodiagnostic Company, Dokki, Giza, Egypt

to the geometrical changes. The fast exchange of ligand coordinated axially to the central metal ion and limited steric hindrance to the approach of the $O_2^{-\cdot}$ anion are considered essential requirements for the successful binding of the $O_2^{-\cdot}$. The flexibility of the metal complex to geometrical arrangement changes [75, 76], during the redox cycling of $M^{n+/}M^{-1}$, which facilitates the interaction of the $O_2^{-\cdot}$ is also important. In addition, the nature of coordinated ligands to the metal ion is also playing an important role in enhancing the SOD like catalytic activity of the SOD functional models [77].

4 Conclusion

The reaction of nickel(II) chloride with both 2-Mercapto-1-isopropylimidazole (Tm^{ipr}) and hydrotris(2-mercapto-1-xylyl-imidazolyl)hydroborate (Tt^{xylyl}) gave two new nickel(II) complexes $[Ni(Tm^{ipr})_2Cl_2]$ **1** and $[Ni(Tt^{xyly})_2]$ **2**, respectively. Tetrahedral geometry for both complexes has been deduced. XRD studies for complex **2** showed that the coordination geometry around nickel atom is ideally regular tetrahedral with four thione sulfur donors from the two anionic ligands (Tt^{xylyl}). The catalytic activity for the SOD reaction of the title complexes has been demonstrated by in vitro measurements, with IC_{50} values of 8.38 and 7.4 mM for complexes **1** and **2**, respectively.

Acknowledgements This work was financially supported by Taif University, Saudi Arabia, Project No.: 1-437-5309.

References

1. D. Fusco, G. Colloca, M.R.L. Monaco, M. Cesari, Clin. Interv. Aging **2**, 377 (2007)
2. B. Poljsak, Oxidative Med. Cell. Longev. **2011**, 1 (2011)
3. W. Dröge, Physiol. Rev. **82**, 47 (2002)
4. B. Uttara, A.V. Singh, P. Zamboni, R.T. Mahajan, Curr. Neuropharmacol. **7**, 65 (2009).
5. P. Pacherm, J.S. Beckman, L. Liaudet, Physiol. Rev. **87**, 315 (2007)
6. J. Zhao, Plant Signal Behav. **2**, 544 (2007)
7. V. Lobo, A. Patil, A. Phatak, N. Chandra, Pharmacogn. Rev. **4**, 118 (2010).
8. S.R. Maxwell, Drugs **9**, 345 (1995)
9. A. Camins, F. Junyent, E. Verdaguer, C. Beas-Zarate, A.E. Rojas-Mayorquín, D. Ortuño-Sahagún, M. Pallàs, Pharmaceuticals (Basel) **2**, 194 (2009)
10. S.C. Shivhare, A.O. Patidar, K.G. Malviya, K.K. Shivhare-Malviya, Ayu **32**, 388 (2011)
11. H.S. Buttar, T. Li, N. Ravi, Exp. Clin. Cardiol. **10**, 229 (2005)
12. S.L. Mehta, Y. Lin, W. Chen, F. Yu, L. Cao, Q. He, P.H. Chan, P.A. Li, Transl. Stroke Res. **2**, 42 (2011)
13. S.W. Ragsdale, J. Biol. Chem. **284**, 18571 (1999)
14. K.C. Ryan, A.I. Guce, O.E. Johnson, T.C. Brunold, D.E. Cabelli, S.C. Garman, M.J. Maroney, Biochemistry **54**, 1016 (2015)
15. B. Palenic, B. Brahamsha, F.W. Larimer, M. Land, L. Hauser, P. Chain, J. Lamerdin, W. Regala, E.E. Allen, J. McCarren, I. Paulsen, A. Dufresne, F. Partensky, E.A. Webb, J. Waterbury, Nature **424**, 1037 (2003)
16. S.B. Choudhury, J.W. Lee, G. Davidson, Y.I. Yim, K. Bose, M.L. Sharma, S.O. Kang, D.E. Cabelli, M.J. Maroney, Biochemistry **38**, 3744 (1999).
17. D.J. Wuerges, J.-W. Lee, Y.-I. Yim, H.-S. Yim, S.-O. Kang, K.D. Carugo, Proc. Natl. Acad. Sci. USA **101**, 8569 (2004)
18. Z. Xu, S. Pan, G. Li, Y. He, R. Wang, J. Inorg. Organomet. Polym. **25**, 1313 (2015)
19. G. Yan, Y. He, G. Li, Y. Xiong, P. Song, R. Wang, J. Chem. Sci. **11**, 1783 (2016)
20. G. Li, H. Zhang, R. Wang, Y. Feng, H. Yu, B. Xiong, Chin. Sci. Bull. **58**, 2956 (2013)
21. S.K. Chatterjee, R.C. Maji, S.K. Barman, M.M. Olmstead, A.K. Patra, Angew. Chem. Int. Ed. Engl. **53**, 10184 (2014)
22. D. Nakane, Y. Wasada-Tsutsui, Y. Funahashi, T. Hatanaka, T. Ozawa, H. Masuda, Inorg. Chem. **53**, 6512 (2014)
23. A. Prokop, J.M. Davidson, J. Pharm. Sci. **9**, 3518 (2008)
24. I. Batinić-Haberle, J.S. Rebouças, I. Spasojević, Antioxid. Redox Signal **13**, 877 (2010)
25. M.M. Ibrahim, A.M. Ramadan, G.A.M. Mersal, S.A. El-Shazly, J. Mol. Struct. **998**, 1 (2011)
26. A.M. Ramadan, M.M. Ibrahim, S.Y. Shaban, J. Mol. Struct. **1006**, 348 (2011)
27. S.Y. Shaban, A.M. Ramadan, M.M. Ibrahim, M.A. Mohamed, R. Van Eldik, Dalton Trans. **44**, 14110 (2015)
28. M.M. Ibrahim, A.M. Ramadan, M.A. Mohamed, M. Soliman, S.I.M. Zayed, J. Coord. Chem. **18**, 4296 (2015)
29. A.M. Ramadan, J. Mol. Struct. **1015**, 56 (2012)
30. A.M. Ramadan, J. Coord. Chem. **65**(8), 1417 (2012)
31. M.M.M. Ibrahim, S.Y. Shaban, Inorg. Chim. Acta **362**, 1471 (2009)
32. M.M. Ibrahim, J. Mol. Struct. **937**, 50 (2009)
33. M.M. Ibrahim, C.P. Olmo, T. Tekeste, J. Seebacher, G. He, J.A.M. Calvo, K. Böhmerle, G. Steinfeld, H. Brombacher, H. Vahrenkamp, Inorg. Chem. **45**, 7493 (2006)
34. M.M. Ibrahim, J. Seebacher, G. Steinfeld, H. Vahrenkamp, Inorg. Chem. **44**, 8531 (2005)

35. M.M. Ibrahim, G. He, J. Seebacher, B. Benkmil, H. Vahrenkamp, Eur. J. Inorg. Chem. **2005**, 4070–4077 (2005)
36. SAINT, V6.02, BrukerAXS, Madison, WI (1999)
37. G.M. Sheldrick, SADABS, Area-Detector Absorption Correction, Göttingen, Germany (1996)
38. G.M. Sheldrick, SHELXL2013. University of Göttingen, Germany (2013)
39. L. Lutterotti, MAUD, CPD, Newsletter (IUCr) 24 (2000)
40. M. Nishikimi, N.A. Roa, K. Yogi, Biochem. Biophys. Res. Commun. **46**, 849–854 (1972)
41. A.M. Ramadan, R.M. Issa, Trans. Met. Chem. **30**, 529 (2005)
42. P.N. Patel, K.K. Shukla, A. Singh, D.K. Patel, J. Niclos-Gutierrez, D. Choquerillo-Lazarte, J. Coord. Chem. **63**, 3648 (2010)
43. M. Chun, S. Lee, S. Yang, J. Colloid Interface Sci. **266**, 120 (2003)
44. R. Shunmugam, D. Sathyanarayana, J. Coord. Chem. **12**, 151 (1983)
45. E.S. Raper, J.L. Books, J. Inorg. Nucl. Chem. **39**, 2163 (1977).
46. L.J. Bellamy, *The infrared spectra of complex molecules*, 3rd edn. (Chapman and Hall, London, 1975)
47. E.S. Raper, P.H. Crackett, Inorg. Chim. Acta **50**, 159 (1981)
48. M.O. Albers, S.F.A. Crosby, D.C. Liles, D.J. Robinson, A. Shaver, E. Singleton, Organometallics **6**, 2014 (1987)
49. J.C. Bommer, K.W. Morse, J. Am. Chem. Soc. **96**, 6222 (1974)
50. J.C. Bommer, K.W. Morse, Inorg. Chem. **19**, 587 (1980)
51. G.G. Lobbia, C. Pettinari, C. Santini, N. Somers, B.W. Skelton, A.H. White, Inorg. Chim. Acta **319**, 15 (2001)
52. P.D. Bailey, A. Dawson, C. McCormack, S.A. Moggach, I.D.H. Oswald, D.W.H. Rankin, A. Turner, Inorg. Chem. **44**, 8884 (2005)
53. D.V. Patel, J. Mihalcik, K.A. Kreisel, G.P.A. Yap, L.N. Zakharov, W.S. Kassel, A.L. Rheingold, D. Rabinovich, Dalton Trans. **14**, 2410 (2005)
54. M. Careri, L. Elviri, M. Lanfranchi, L. Marchiò, C. Mora, M.A. Pellinghelli, Inorg. Chem. **42**, 2109 (2003)
55. R. Cammi, M. Gennari, M. Giannetto, M. Lanfranchi, L. Marchiò, G. Morri, C. Paiola, M.A. Pellinghelli, Inorg. Chem. **44**, 433 (2005)
56. S. Kiani, J.R. Long, P. Stavropoulos, Inorg. Chim. Acta **263**, 357 (1997)
57. M. Gennari, M. Lanfranchi, L. Marchiò, M.A. Pellinghelli, M. Tegoni, R. Cammi, Inorg. Chem. **45**, 3456 (2006)
58. H. Takeuchi, I. Harada, Spectrochim. Acta **49**, 1069 (1986).
59. R.L. Dutta, A. Syamal, *Elements of magnetochemistry*, 2nd edn. (Affiliated East-West Press, Delhi, 2007)
60. B.N. Figgis, J. Lewis, Prog. Inorg. Chem. **6**, 37 (1964)
61. A.B.P. Lever, *Inorganic electronic spectroscopy*, 2nd edn. (Elsevier, Amsterdam, 1984)
62. M. Amirnasr, A.H. Mahmoudkhani, A. Gorji, S. Dehghanpour, H.R. Bijanzadeh, Polyhedron **21**, 2733 (2002)
63. H.A. Bayoumi, A.M.A. Alaghaz, M.S. Aljahdali, Int. J. Electrochem. Sci. **8**, 9399 (2013)
64. B.M. Bridgewater, T. Fillebeen, R.A. Friesner, G. Parkin, J. Chem. Soc. Dalton Trans. **24**, 4494 (2000)
65. C. Kimblin, B.M. Bridgewater, D.G. Churchill, T. Hascall, G. Parkin, Inorg. Chem. **39**, 4240 (2000)
66. H. Vahrenkamp, Acc. Chem. Res. **32**, 589 (1999)
67. M. Tesmer, M. Shu, H. Vahrenkamp, Inorg. Chem. **40**, 4022 (2001)
68. M.M. Ibrahim, G.A.M. Mersal, S. Al-Juaid, S. El-Shazly, J. Mol. Struct. **166**, 1056 (2014)
69. M.M. Ibrahim, S.S. Al-Juaid, Q. Mohsen, Phosphorus Sulfur Silicon **184**, 2324 (2009)
70. G. Ischia, H.-R. Wenk, L. Lutterotti, F. Berberich, Quantitative Rietveld texture analysis from single synchrotron diffraction images. J. Appl. Cryst. **38**, 377 (2005)
71. J.R.J. Sorenson (Ed.), *Inflammatory diseases and copper*, Humana Press, Clifton, 1982)
72. J.R.J. Sorenson, in *Metal ions in biological systems*, vol. 14, ed. by H. Sigel (Marcel Dekker, New York, 1982), p. 77
73. R.N. Patel, N. Singh, K.K. Shukla, V.L.N. Gundla, U.K. Chauhan, Spectrochim. Acta A **63**, 21 (2006)
74. H.D. Youn, E.J. Kim, J.H. Roe, Y.C. Hah, S.O. Kang, Biochem. J. **318**, 889 (1996)
75. S.L. Lippard, J. M. Berg, *Principles of bioinorganic chemistry*. (University Science Books, Mill Valley, 1994)
76. E.J. Baran, *Qumica bioinorganica*. (McGraw-Hill Interamericana de Espana S, McGraw-Hill Interamericana de Espana S.A, Madrid, 1995)
77. A.L. Abuhijleh, J. Khalaf, Eur. J. Med. Chem. **45**, 3811 (2010)